4) The spatial extent of the surface deformation at tilt sensitivities of 10^{-7} radian rarely exceeds 10 *S*.

The simple model of deep aseismic slip along the fault, as indicated, for example, by the observed broad-scale heat flow anomaly (*12*), which has associated shallow seismicity and local crustal deformation effects, could explain some of the tilt observations.

It is difficult to use these observations to argue either for or against currently popular ideas of the dilatancy behavior of crustal rocks since tilts of either sense could result from dilatancy by causing variations in the depth of the dilatant region or by causing interaction with the stress fields around the fault. The simple form of large-scale positive crustal swelling does appear unlikely for the earthquakes we have seen. As more data become available, it will be possible to determine more uniquely details of the earthquake mechanism, in particular, whether similar effects occur for larger-magnitude ranges and for different locations.

M. J. S. JOHNSTON
C. E. MORTENSEN

U.S. Geological Survey, National Center for Earthquake Research, Menlo Park, California 94025

References and Notes

1. F. Press and W. F. Brace, *Science* **152**, 1575 (1966); T. Hagiwara and T. Rikitake, *ibid.* **157**, 761 (1967); T. Rikitake, *Tectonophysics* **6**, 1 (1968); E. F. Saverensky, *ibid.*, p. 17.
2. Y. P. Aggarwal, L. R. Sykes, J. Armbruster, M. L. Sbar, *Nature (Lond.)* **241**, 101 (1973); I. N. Gupta, *Trans. Am. Geophys. Union* **55**, 355 (1974); R. Robinson, R. L. Wesson, W. L. Ellsworth, *Science* **184**, 1281 (1974).
3. J. H. Whitcomb, J. D. Garmany, D. L. Anderson, *Science* **180**, 632 (1973).
4. A. Nur, *Bull. Seismol. Soc. Am.* **62**, 1217 (1972); C. H. Scholz, L. R. Sykes, Y. P. Aggarwal, *Science* **181**, 803 (1973).
5. M. A. Chinnery, *Bull. Seismol. Soc. Am.* **51**, 9 (1961); J. C. Savage, *J. Geophys. Res.* **76**, 1954 (1971).
6. C. E. Mortensen and M. J. S. Johnston, in preparation.
7. These units are manufactured commercially by the Autonetic Division of North American Rockwell, model 541B.
8. The installation procedure is similar to that described by R. V. Allen, D. M. Wood, and C. E. Mortensen [*Philos. Trans. R. Soc. Lond. Ser. A Math. Phys. Sci.* **274**, 219 (1973)].
9. M. J. S. Johnston, in preparation.
10. Estimates of source dimension as a function of earthquake magnitude have been made by M. Wyss and J. Brune [*Bull. Seismol. Soc. Am.* **61**, 1153 (1971)], and observations for San Andreas earthquakes have been made by W. Thatcher and T. Hanks [*J. Geophys. Res.* **78**, 8547 (1973)].
11. Very careful checking is necessary with this type of data to ensure that there is no possibility of an earthquake-induced instrumental effect.
12. A. H. Lachenbruch and J. H. Sass, in *Proceedings of the Conference on Tectonic Problems of the San Andreas Fault System*, R. L. Kovach and A. Nur, Eds. (Stanford Univ. Press, Stanford, Calif., 1973), p. 192.
13. We thank R. Allen and others at the National Center for Earthquake Research for useful suggestions and help.

15 July 1974

Aerosols in the Atmosphere: Calculation of the Critical Absorption/Backscatter Ratio

Abstract. *The ratio of the absorption coefficient to the backscatter coefficient for which heating and cooling effects due to aerosols exactly balance at the earth's surface has been calculated with the use of a radiative-convective atmospheric model. The results are compared with those obtained from several simpler mean radiative-transfer models.*

In this report a radiative-convective atmospheric (RCA) model (*1*, *2*) is used to calculate the value of the aerosol extinction coefficient and also the magnitude of the critical aerosol absorption/backscatter ratio for which heating and cooling effects due to aerosols just balance to produce no net temperature change at the earth's surface. These quantities are calculated for three aerosol heights. The RCA critical ratios are compared with several other recent calculations obtained from simple mean radiative-transfer (MRT) models (*3*–*5*).

The RCA model results confirm (*2*, *6*) that an aerosol layer in the atmosphere changes the radiative balance and produces two effects in the atmosphere: (i) an increase in the mean earth-atmosphere albedo (a cooling effect) and (ii) a reduction of the atmospheric radiative cooling (a heating effect). The aerosol backscatter of incoming solar radiation increases the earth-atmosphere albedo while the absorption of the solar radiation increases the atmospheric temperature (and thus reducing the net radiative cooling).

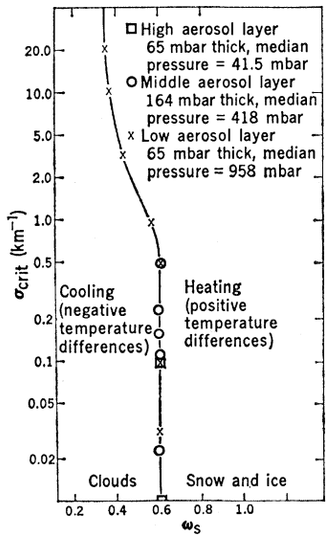

Fig. 1. Calculated RCA values of the critical aerosol extinction coefficient in the visible, σ_{crit}, as a function of the mean shortwave surface albedo, ω_s. The aerosol layer height (in millibars) is the median height for the particles.

The RCA model was developed by Manabe and Wetherald (*1*), and I have modified it to include an aerosol layer (*2*). A forward time integration of the solar and terrestrial flux imbalance is carried out until a radiative-convective, steady-state temperature is asymptotically approached at each of nine vertically aligned points in the atmosphere. A three-layer water cloud distribution with the appropriate optical properties (the same as that used by Manabe and Wetherald) is used to represent the clouds at 35°N in April. The physical distributions of H_2O, CO_2, and O_3 used by Manabe and Wetherald are also assumed, so that their necessary radiative-transfer effects can be included. The input aerosol optical parameters are similar to those previously used by Rasool and Schneider (*7*) for the global average aerosol. Parameterized expressions (*2*) are used to calculate (in a two-stream approximation) the fraction of transmitted and backscattered radiation due to the presence of the aerosol layer at various heights. Mie scattering is assumed for individual particles with a mean visible refractive index of $m = 1.50 - 0.1\ i$, an inverse fourth-power distribution of the particle radius, and a ratio of the mean extinction coefficient in the visible (0.55 μm) to that in the infrared (10 μm) of 0.108. Details of this model are given in (*2*). Earlier RCA model calculations (*2*) have shown that aerosols cause cooling at the earth's surface when the surface albedo, ω_s, is small ($\omega_s = 0.07$, as over water) and heating when the surface albedo is large ($\omega_s \geq 0.6$, as over snow).

These same calculations indicate that there is a value of the aerosol visible extinction coefficient, σ_{crit}, for which no heating or cooling occurs at the surface. This RCA model was used to compute the dependence of σ_{crit} on ω_s in the following way. A range of extinction coefficients, σ, and ω_s values was arbitrarily chosen,

and a value of ΔT_s (the difference in the surface temperature with and without aerosols) was calculated for each set of σ and ω_s values. For a fixed value of σ, the relationship between ω_s and ΔT_s was found to determine whether there was a value of ω_s for which $\Delta T_s \to 0$. In this case σ becomes σ_{crit} for that value of ω_s. The results are given in Fig. 1.

In the calculation the high and low aerosol layers are each 65 mbar thick. The middle aerosol layer is 164 mbar thick. These aerosol layer thicknesses were held constant, and the optical depth and σ were changed by changing the number density of particles in these layers. Moreover, within an aerosol layer, the aerosol number density scales according to the barometric pressure.

Since Rasool and Schneider did not determine σ_{crit} for their global average model, these results cannot be compared directly with their work. However, their calculation corresponded to a surface albedo of about 0.1 (the global average value), and so their computations fall in the strong cooling regime of this work. Indeed, their work, which was restricted to the one surface albedo, did predict a sizable cooling effect due to aerosols.

In the region to the left of the curve (Fig. 1), corresponding to smaller values of the surface albedo, cooling occurs, whereas in the region to the right of the curve, corresponding to larger values of the surface albedo, heating occurs. Additional calculations for larger extinction coefficients (*2*) indicate that $\sigma_{crit} \to \infty$ as $\omega_s \to 0.35$. Thus, for the aerosols in this model the cooling and heating effects at the surface can balance only over surfaces having albedos in the range 0.35 to 0.60. For $\omega_s > 0.6$ heating always occurs, and for $\omega_s < 0.35$ cooling always occurs. In addition, it is only when σ is greater than ten times the present mean background level (~ 0.065 to 0.1 km^{-1}) that heating can ever occur over surfaces that have albedos of less than 0.6.

A single test was carried out to determine the sensitivity of these results to variations in the ratio of the mean aerosol infrared extinction coefficient to the visible extinction coefficient. For an aerosol layer at a median pressure of 958 mbar and for a σ_{crit} of 1 km^{-1} an increase of a factor of 2 in the infrared extinction coefficient relative to the visible extinction coefficient changed the ω_s value by only ~ 1 percent (0.575 to 0.570).

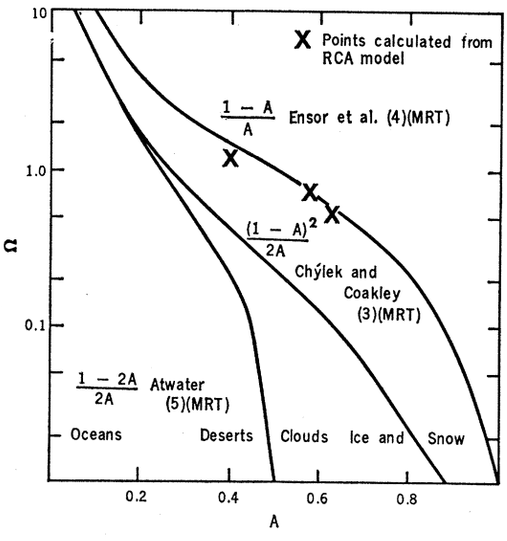

Fig. 2. Calculated values of the critical ratio of the aerosol absorption cross section to the average backscatter cross section Ω (for visible light) given as a function of the mean shortwave earth-atmosphere albedo, A. [Atwater (*5*) and Ensor *et al.* (*4*) indicate that A is the surface albedo, but the manner in which the expressions are derived indicates that the A used is the total earth-atmosphere albedo without the particles. For Chýlek and Coakley (*3*) and in this report A is the albedo of the underlying earth-atmosphere system.]

From the results shown in Fig. 1 it appears the relationship between σ_{crit} and ω_s is independent of the altitude of the aerosol layer—at least where calculations for all heights are possible. For high and middle aerosol layers, only the smaller values of the extinction coefficient are physically reasonable; larger values of σ would correspond to unrealistically large particle densities at the higher altitudes. However, I do find coincident σ_{crit} values for both high and middle aerosol layers at $\sigma_{crit} = 0.1$ km^{-1}. For $\sigma_{crit} < 0.5$ km^{-1} this result implies that neither the stratospheric nor the tropospheric aerosol layers produce any surface temperature effects over surface albedos of 0.6.

It should be stressed that the results presented here assume "averaged" aerosol properties and pertain only to the present RCA model. Yet to be established is the degree to which these results would depend on changes in (i) the visible scattering and absorption efficiencies of the aerosol, (ii) the aerosol size distribution, and (iii) the abundance and optical properties of water clouds.

Let us now turn to a comparison of the results with the MRT models (Fig. 2). The critical ratio Ω (the ratio of the visible absorption cross section to the average visible backscattering cross section of the aerosol) is plotted as a function of the mean earth-atmosphere albedo, A (rather than ω_s as in Fig. 1). For the RCA model Ω corresponds to the situation for which the aerosol layer, when added to the earth-atmosphere system, produces no net *surface* temperature change (the value of A for which $\Delta T_s \to 0$). Also shown are the numerical MRT results of Chýlek and Coakley (*3*), Atwater (*5*), and Ensor *et al.* (*4*). The MRT calculations determine the effect on the planetary albedo due to the addition of an aerosol layer; hence they refer to the heating or cooling of the *entire* earth-atmosphere system rather than the heating or cooling at the surface. To the extent that the RCA and MRT models can be compared, the numerical results from the RCA model are closest to those of Ensor *et al.* (*4*).

In the most recent study, Chýlek and Coakley (*3*) assume (at a given optical depth) a constant isotropic upward and downward intensity and thereby are able to obtain an analytic approximation to the solution of the radiative-transfer equation. From their model they conclude that the sign of the heating (that is, heating or cooling) is independent of the optical thickness of the aerosol layer, and that the amount of heating approaches a finite limit with the increasing thickness of the aerosol layer. The results of the RCA model (*2*) are in qualitative agreement on this point with those from this MRT model (*3*). Hence I conclude that this simpler MRT model is sufficient to determine both the sign and the fact of a finite limit to the heating effect.

RUTH A. RECK

Physics Department,
General Motors Research Laboratories,
Warren, Michigan 48090

References and Notes

1. S. Manabe and R. T. Wetherald, *J. Atmos. Sci.* **24**, 241 (1967).
2. R. A. Reck, *Atmos. Environ.* **8**, 823 (1974); *ibid.*, in press.
3. P. Chýlek and J. A. Coakley, Jr., *Science* **183**, 75 (1974).
4. D. S. Ensor, W. M. Porch, M. J. Pilot, R. J. Charlson, *J. Appl. Meteorol.* **10**, 1303 (1971).
5. M. A. Atwater, *Science* **170**, 64 (1970).
6. W. D. Sellers, *Physical Climatology* (Univ. of Chicago Press, Chicago, ed. 3, 1969), p. 5.
7. S. I. Rasool and S. H. Schneider, *Science* **173**, 138 (1971).

8. I thank R. T. Wetherald and S. Manabe of the Geophysical Fluid Dynamics Laboratory, National Oceanic and Atmospheric Administration, at Princeton University for a copy of their RCA code into which I have introduced the role of particulate aerosols.

8 April 1974; revised 9 August 1974 ■

Electron Diffraction of Frozen, Hydrated Protein Crystals

Abstract. *High-resolution electron diffraction patterns have been obtained from frozen, hydrated catalase crystals to demonstrate the feasibility of using a frozen-specimen hydration technique. The use of frozen specimens to maintain the hydration of complex biological structures has certain advantages over previously developed liquid hydration techniques.*

There is great potential for the use of electron microscopy to investigate the structures of complex biological objects at high resolution. However, if high-resolution structure is to be observed, either by electron diffraction or by direct imaging, the specimen must be maintained in a hydrated condition in the high vacuum of the electron microscope. Until recently this was not possible because techniques were not available for maintaining the hydration of the native biological structure. To overcome the hydration problem, previous investigators have used (i) closed cell, thin window environmental chambers and (ii) differentially pumped hydration stages (*1*). A high degree of success has been achieved with differentially pumped stages by Parsons and co-workers, who obtained electron diffraction patterns from unstained, unfixed catalase crystals in the hydrated state (*2*) and from wet, human erythrocyte membranes (*3*). Catalase crystals are convenient specimens for testing hydration efficiency because the protein is easily crystallizable as thin plates suitable for electron diffraction, and its diffraction pattern is sensitive to hydration effects (*2*, *4*).

We have been exploring the feasibility of using frozen specimens as an alternative method of maintaining specimen hydration. We have now obtained electron diffraction patterns from frozen, unstained, unfixed catalase crystals sandwiched between thin, hydrophilic support films.

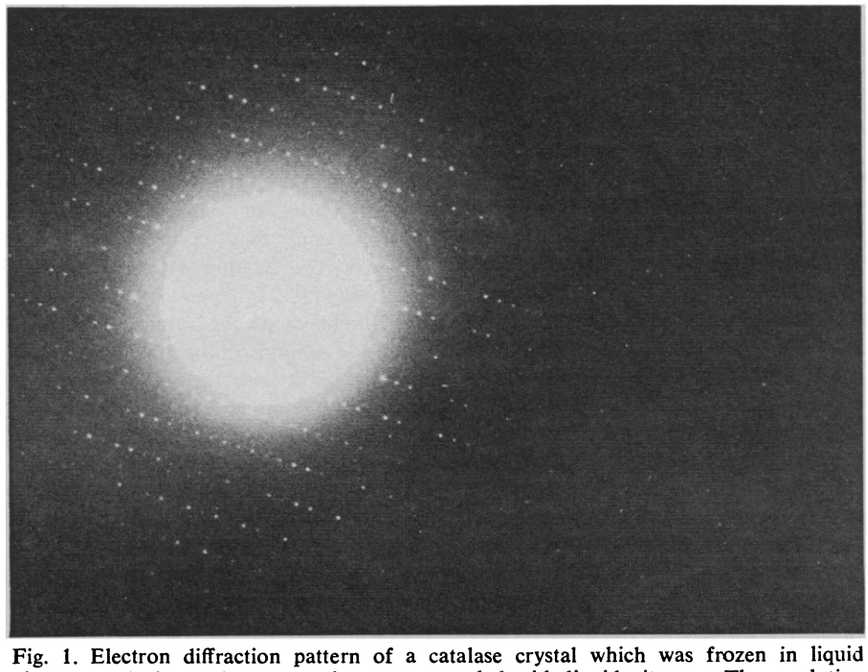

Fig. 1. Electron diffraction pattern of a catalase crystal which was frozen in liquid nitrogen and observed on a specimen stage cooled with liquid nitrogen. The resolution of the photographic reproduction is 4.5 Å, although that of the diffraction pattern on the original plate was 3.4 Å.

Catalase crystals suitable for electron diffraction were prepared as described by Wrigley (*5*). Specimens for electron diffraction were prepared from suspensions of the very thin plate crystals, which were placed between thin, hydrophilic support films by the capillary action effect; the specimens were frozen as described in (*6*). Frozen specimens were introduced into the microscope vacuum of a JEM 100B electron microscope by using a combined cold sink and frost protector mounted in the airlock door. Selected area diffraction patterns were obtained with current densities at the specimen of approximately 10^{-5} ampere/cm^2, a diffraction camera length of 3.8 m, and an accelerating voltage of 100 kev. In these conditions the low angle diffraction pattern is easily visible on the fluorescent screen out to the third order of the 70-Å unit cell dimension. The diffraction patterns were recorded on Kodak electron image plates and developed in Kodak HRP developer mixed with water (1 : 2).

Figure 1 shows an electron diffraction pattern obtained from a frozen catalase crystal; the resolution in the photograph is 4.5 Å. Electron diffraction patterns with resolutions of 3.4 Å have been obtained on plates, but are difficult to reproduce photographically. Because of the relatively slow electron speed of the conventional electron image plates, specimen electron exposures of the order of 10^{-3} coulomb/cm^2 were necessary in order to record the diffraction patterns. However, even after such doses the low-resolution pattern remained unchanged. Quantitative measurements of the critical dose for loss of crystalline diffraction as a function of resolution have been made (*7*).

The demonstration that crystalline order is retained in protein crystals directly frozen in liquid nitrogen, without the use of cryoprotectants, is important for establishing the feasibility of using frozen specimens for maintaining hydration. There was ample reason to believe, both from results with freeze fracture and with techniques for preparing frozen thin sections and from unpublished early x-ray diffraction experiments, that severe disorder of biological structure could occur during direct freezing in liquid nitrogen. Our results show that this is not necessarily the case for specimens of the size and thickness used for electron microscopy.

There are several reasons for using